

## Article

# Computational Fluid Dynamics Simulation of Filling a Hydrogen Type 3 Tank at a Constant Mass Flow Rate

José Miguel Monteiro <sup>1</sup>, Leonardo Ribeiro <sup>1,2</sup>, Joaquim Monteiro <sup>1,2</sup>, Andresa Baptista <sup>1,2</sup>  
and Gustavo F. Pinto <sup>1,2,\*</sup>

<sup>1</sup> ISEP—School of Engineering, Polytechnic of Porto, Rua Dr. António Bernardino de Almeida, 4249-015 Porto, Portugal; 1170674@isep.ipp.pt (J.M.M.); lsr@isep.ipp.pt (L.R.); jfmo@isep.ipp.pt (J.M.); absa@isep.ipp.pt (A.B.)

<sup>2</sup> INEGI—Institute of Science and Innovation in Mechanical and Industrial Engineering, 4200-465 Porto, Portugal

\* Correspondence: gflp@isep.ipp.pt

**Abstract:** Hydrogen storage in high-pressure tanks can be performed with different filling strategies. Many studies have been carried out on supplies with increasing pressure rates. The present work aims to carry out CFD numerical simulations, using Ansys Fluent<sup>®</sup>, in a type 3 tank of 70 MPa normal working pressure (NWP) using a constant flow rate, to analyze the influence of inlet key parameters such as initial temperature, mass flow rate, and material properties on the evolution of temperature, pressure, and velocity. From the analysis of the results, it was possible to discover linear relationships between the increase in the total equilibrium temperature and the final hydrogen temperature, as well as a linear increasing relationship between inlet and final temperatures when the equilibrium temperature was fixed. Considering fully adiabatic walls resulted in a significant increase in temperature with no predictable pattern. The difference between total and static temperatures found in the inlet tube decreased with the decrease in mass flow rate and subsequently the Mach number. The choice of a polymer for the tank lining led to higher temperatures when compared to an aluminum lining.

**Keywords:** hydrogen filling; type 3 tank storage; CFD numerical simulation; constant mass flow rate



**Citation:** Monteiro, J.M.; Ribeiro, L.; Monteiro, J.; Baptista, A.; Pinto, G.F. Computational Fluid Dynamics Simulation of Filling a Hydrogen Type 3 Tank at a Constant Mass Flow Rate.

*Energies* **2024**, *17*, 1375. <https://doi.org/10.3390/en17061375>

Academic Editors: Giovanni Esposito and Orlando Ayala

Received: 9 February 2024

Revised: 23 February 2024

Accepted: 11 March 2024

Published: 13 March 2024



**Copyright:** © 2024 by the authors. Licensee MDPI, Basel, Switzerland. This article is an open access article distributed under the terms and conditions of the Creative Commons Attribution (CC BY) license (<https://creativecommons.org/licenses/by/4.0/>).

## 1. Introduction

The growing need to reduce greenhouse gas emissions has driven the search for new technologies with the capacity to supply and store large amounts of energy at competitive prices. At the current rate of fossil fuel use, it is expected that, by 2050, their scarcity or economic unfeasibility of extraction will have a strong impact on the world economy [1]. An increase in energy consumption of 50% is predicted between 2018 and 2050, with renewable energy increasing by 3.1% per year, oil by 0.6%, and natural gas by 1.1% [2]. Hydrogen currently represents just 0.03% of global energy production and 2% in Europe. Approximately 96% of this hydrogen is produced from natural gas and is mostly used to produce ammonia and plastics, in hydrotreating processes in oil refineries, and for other chemical products [3]. To be competitive with current technologies, hydrogen supply must meet three goals [3]: low fueling time requirements, high safety, and high filling rates. To this extent, hydrogen supply at stations is carried out according to protocols developed by the Society of Automotive Engineers (SAE) to guarantee the safety and maximum performance of the operation. SAE J2601 aims for the rapid storage (3–5 min) of hydrogen in 35 and 70 MPa normal working pressure (NWP) tanks, up to a high state of charge (90 to 100% state of charge—SOC) and without violating system temperature limits, pressure, and mass flow [4]. The established safety limits are a minimum hydrogen temperature of  $-40\text{ }^{\circ}\text{C}$  and maximum of  $85\text{ }^{\circ}\text{C}$ , maximum pressure supplied of 25% above the NWP, and maximum mass flow of  $0.060\text{ kg}\cdot\text{s}^{-1}$ . These limits prevent the materials'

integrity from being affected. To ensure safety when filling a tank with hydrogen [5–7], it is important to know the phenomena responsible for the increase in temperature. The three most significant factors are (a) the conversion of the gas's kinetic energy into internal energy, (b) the Joule–Thomson effect, and (c) gas compression. The Joule–Thomson effect refers to the heating or cooling of a gas (or liquid) under the influence of large pressure gradients in an adiabatic and isenthalpic flow. This effect is typical in the presence of throttling valves and causes heating in gases with a negative Joule–Thomson coefficient [8]. Hydrogen belongs to the gas group that suffers from this effect.

Hydrogen can be stored in a solid, liquid, or gaseous state. The most common method, especially for storage in light or heavy vehicles, is in the gaseous state. Due to its low density, it is necessary to compress hydrogen at high pressures. Table 1 presents the types of tanks currently available, as well as their construction materials, cost, and properties.

**Table 1.** Types of hydrogen tanks (adapted from [9–11]).

| Type   | Materials   | Pressure Range | Features   |
|--------|---|----------------|--|
| Type 1 | All metal (steel and aluminum)  | 17.5–20        | Heavy, internal corrosion.   |
| Type 2 | Metal liner with hoop wrapping  | 26.3–30        | Heavy, internal corrosion.   |
| Type 3 | Metal liner (aluminum) with full composite wrapping (carbon fiber)        | 35–70          | Lightness, low permeation, galvanic corrosion between liner and fiber, high burst pressure.            |
| Type 4 | Polymer (thermoplastic) liner with full composite wrapping (carbon fiber) | 35–70          | Lightness, high permeation, relatively low burst pressure, no creep fatigue, simple manufacturability. |

Several studies have been carried out to evaluate the fast filling of hydrogen. R. Hirotani et al. [12] demonstrated that tanks with materials with lower thermal conductivity, such as the polymer in type 4 tanks, result in higher temperatures. S.C. Kim et al. [13] found a greater occurrence of stratification in type 4 tanks and that this phenomenon significantly increased the maximum hydrogen temperature. Y. Zhao et al. [14] simulated several patterns of pressure increase and concluded that a linear pattern is the most suitable for obtaining lower final and maximum temperatures. Y.-L. Liu et al. [15] concluded that linear increases in initial pressures result in a linear decrease in maximum temperature. J. Zheng et al. [16] found that there is a linear relationship of temperature increase between the equilibrium temperature and final temperature. M. C. Galassi et al. [17] simulated a fully adiabatic tank and found that it resulted in significant increases in maximum and final temperature. N. de Miguel et al. [18] demonstrated that an increase in diameter and decrease in mass flow rate caused the formation of stratification due to low velocities. N. R. Kesana et al. [19] modeled a tank with a high length-to-diameter ratio and found that, in this type of tank, buoyancy effects are significant. D. Melideo et al. [20] concluded that the drop in final temperature is approximately equal in magnitude to the same drop in precooling temperature. Wang G et al. [21] determined that the final mass of hydrogen is inversely proportional to the mass flow rate and depends on heat transfer during fueling. Also was constructed a nonlinear curve that fits the decrease in final mass with the increase in mass filling rate in a 35 MPa type 3 tank. On the other hand, the final mass increased linearly with the increase in initial pressure. R. Cebolla et al. [22] demonstrated that the higher the mass flow rate, the lower the SOC, but this tendency decreased with the increase in pre-cooled inlet gas. Decreasing the pre-cooled temperature led to an increase in tank energy content higher than the energy spend.

The present study aims to numerically analyze the rapid filling of hydrogen in a type 3/4 tank of 70 MPa NWP and constant mass flow rate as the inlet condition. The

new relationships found in this article are relevant to better understanding and predicting the thermal behavior of these types of tanks in various conditions. The behavior of key variables such as temperature, pressure, and velocity in different configurations of initial conditions is evaluated. We also present a new insight into the effects of compressibility caused by the high velocity at the inlet, which is, to the best of the authors' knowledge, the first attempt to quantitatively evaluate this effect. The CFD simulation results are verified and validated with the results of D. Melideo et al. [23].

## 2. CFD Simulations

### 2.1. Cases Studied

The geometry (Figure 1) is composed of a cylinder and two half spheres, with dimensions according to Table 2. It was necessary to modify the interior length of the tank due to the lack of information on the exact geometry of the concave areas. The length was changed so that the resulting volume was 40 L. Due to the high computational cost of a 3D simulation, we decided to carry out a 2D simulation. The construction of the 2D geometry was carried out by establishing the X axis as the axis of axial symmetry [24]. The inlet tube had an internal diameter of 3 mm and a thickness of 2 mm.

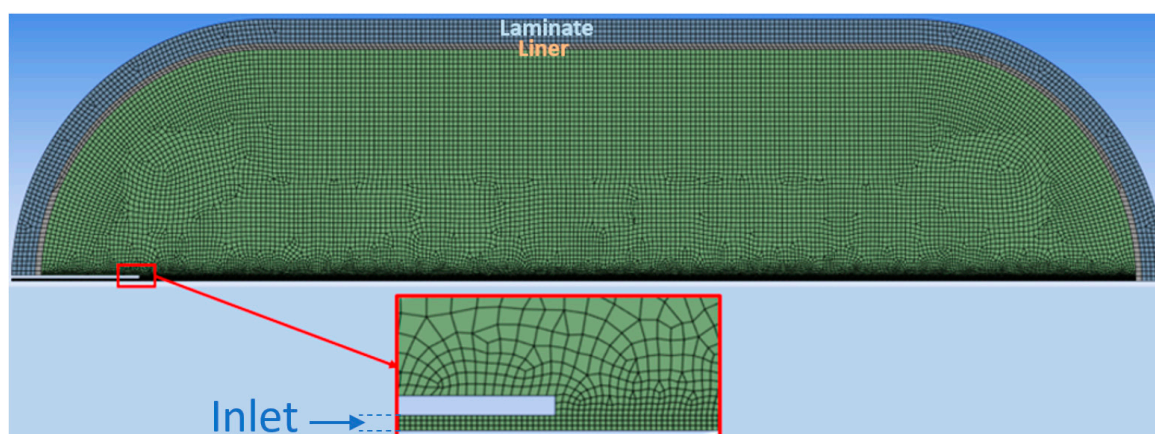


Figure 1. Computational mesh.

Table 2. Dimensions of the tank.

| Internal Length (m) | Inner Radius (m) | Liner Thickness (m) | Laminate Thickness (m) |
|---------------------|------------------|---------------------|------------------------|
| 0.702               | 0.145            | 0.004               | 0.015                  |

The simulations carried out can be seen in Table 3, divided into eight categories to which the cases correspond. This work used the 40 L, 70 MPa type 3 tank (NWP) from the article by D. Melideo et al. [23] for all simulations, as well as their experimental results for the validation, case 1, of the CFD model [25]. The results were also compared between the standard  $K-\epsilon$  turbulence model in case 1 and the realizable  $K-\epsilon$  model in case 2. In cases 3 and 4, the temperature was successively increased by 10 K. An initial condition of thermal equilibrium between the tank, environment, and supplied hydrogen was assumed for case 3, and a fixed initial temperature (279 K) was assumed for case 4. Velocity is a highly important parameter in evaluating the flow behavior and temperatures of hydrogen. As it is interconnected with the mass flow rate, in case 6, different mass flow rates were tested and their impact analyzed. To analyze the influence on temperature associated with the fully adiabatic case, a mesh without lining and coating was constructed, and two sets of simulations were carried out, cases 5 and 7, with initial conditions equal to non-adiabatic cases 3 and 6, respectively. Finally, in case 8, a type 4 tank with a high-density polyethylene polymer (HDPE) lining was simulated, with the same dimensions as type 3 and flow conditions as case 4-C.

Table 3. Parameters of CFD simulations.

| Simulations | Inlet Temperature (K) | Initial Temperature (K) | Mass Flow Rate (kg·s <sup>-1</sup> ) | Exterior Temperature (K) |
|-------------|-----------------------|-------------------------|--------------------------------------|--------------------------|
| Case 1      | UDF                   | 293                     | 0.008                                | 293                      |
| Case 2      | UDF                   | 293                     | 0.008                                | 293                      |
| Case 3-A    | 313                   | 313                     | 0.008                                | 313                      |
| Case 3-B    | 303                   | 303                     | 0.008                                | 303                      |
| Case 3-C    | 293                   | 293                     | 0.008                                | 293                      |
| Case 3-D    | 283                   | 283                     | 0.008                                | 283                      |
| Case 4-A    | 313                   | 279                     | 0.008                                | 313                      |
| Case 4-B    | 303                   | 279                     | 0.008                                | 303                      |
| Case 4-C    | 293                   | 279                     | 0.008                                | 293                      |
| Case 4-D    | 283                   | 279                     | 0.008                                | 283                      |
| Case 5-A    | 303                   | 303                     | 0.008                                | adiabatic                |
| Case 5-B    | 293                   | 293                     | 0.008                                | adiabatic                |
| Case 5-C    | 283                   | 283                     | 0.008                                | adiabatic                |
| Case 6-A    | 293                   | 279                     | 0.01                                 | 293                      |
| Case 6-B    | 293                   | 279                     | 0.006                                | 293                      |
| Case 6-C    | 293                   | 279                     | 0.004                                | 293                      |
| Case 6-D    | 293                   | 279                     | 0.002                                | 293                      |
| Case 7-A    | 293                   | 279                     | 0.008                                | adiabatic                |
| Case 7-B    | 293                   | 279                     | 0.006                                | adiabatic                |
| Case 7-C    | 293                   | 279                     | 0.004                                | adiabatic                |
| Case 8      | 293                   | 279                     | 0.008                                | 293                      |

The Ansys Fluent<sup>®</sup> version 2023 R2 was used as simulation software. Due to the high computational cost, only 50 s was simulated in each case. After carrying out time step independence tests with values of 0.005, 0.002 and 0.001 s, a conservative decision was made to use a time step of 0.002 s in all simulations. The initial pressure value in all simulations was 2 MPa.

## 2.2. Preprocessing Settings

The physical properties of the materials for type 3 and 4 tanks we used can be found in [26]. For hydrogen, specific heat (Cp), thermal conductivity, and dynamic viscosity were established as fourth-degree polynomial functions [27]. The calculation of the density of hydrogen is performed using the equation of state. Due to the high pressures that occur during filling, a real gas equation is indicated. In previous works, it was observed that the equation with the best results was that of Redlich–Kwong [28], given by (1).

$$p = \frac{RT}{V_m - b} - \frac{a}{\sqrt{TV_m}(V_m + b)}, \quad (1)$$

where  $V_m$  is the mole volume,  $R$  the universal gas constant with a value of  $8.314 \text{ J} \cdot \text{mol}^{-1} \cdot \text{K}^{-1}$ ,  $T$  the temperature, and  $a$  and  $b$  are correction constants for the molecular and volumetric attractive potential, respectively. These constants are calculated at the critical pressure  $p_c$  and critical temperature  $T_c$  [29], according to Equation (2).

$$a = \frac{0.42748R^2T_c^{2.5}}{p_c}, b = \frac{0.08664RT_c}{p_c} \quad (2)$$

Three meshes were constructed for mesh independence verification tests and one (mesh 4) for the adiabatic cases. The model used (except case 2) was the standard K-ε. It is a popular, robust model with a relatively low computational cost and which has shown good results according to several authors [8,14,20] as well as in the current validation process. It was necessary to modify the C1 constant from 1.44 to 1.52 due to the high propagation rate of the hydrogen jet, found in this model by [30]. The realizable K-ε model differs from the standard in the formulation of the equation for the turbulent dissipation rate and in C<sub>μ</sub>′, which becomes a variable as opposed to a constant in the standard.

Due to the compression of the gas in the tank, heating by viscous forces cannot be considered negligible, which is why viscous heating was activated [27]. In both models, scalable wall functions were used for the wall treatment. Figure 1 illustrates the computational mesh, structured and non-adaptive of 26522 cells, resulting from the mesh independence tests.

As the inlet tube is adiabatic, its mesh was not constructed. For the adiabatic cases (5 and 7), the outer surface had a condition of zero heat flux (adiabatic). For the remaining cases, a convection condition was established with the value of the heat transfer coefficient equal to 6 W·m<sup>-2</sup>·K<sup>-1</sup> [23].

### 2.3. Governing Equations and Solver Settings

Together with the real gas equation, an equation for the conservation of mass (3), two for momentum (4), and another for energy (5) were solved [31]. A summary of the parameters used for the solver in this work is presented in Table 4.

$$\frac{\partial \rho}{\partial t} + \frac{\partial}{\partial x_i}(\rho u_i) = 0 \tag{3}$$

$$\frac{\partial}{\partial t}(\rho u_i) + \frac{\partial}{\partial x_j}(\rho u_i u_j) = -\frac{\partial p}{\partial x_i} + \frac{\partial}{\partial x_j} \left[ \mu \left( \frac{\partial u_i}{\partial x_j} + \frac{\partial u_j}{\partial x_i} - \frac{2}{3} \delta_{ij} \frac{\partial u_m}{\partial x_m} \right) \right] + \frac{\partial}{\partial x_j} \left( -\rho \overline{u_i' u_j'} \right) \tag{4}$$

$$\frac{\partial}{\partial t}(\rho E) + \frac{\partial}{\partial x_j} (u_j(\rho E + p)) = \frac{\partial}{\partial x_j} \left[ \left( k_h + \frac{C_p \mu_t}{Pr_t} \right) \frac{\partial T}{\partial x_j} + u_i (\tau_{ij})_{eff} \right] \tag{5}$$

where ρ is density, *t* the time, *k<sub>h</sub>* the thermal conductivity, μ and μ<sub>*t*</sub> the viscosity and turbulence viscosity, respectively, *Pr<sub>t</sub>* the turbulent Prandtl number, *p* the pressure, *u* the velocity, *C<sub>p</sub>* the heat capacity at constant pressure, and δ<sub>*ij*</sub> the Kronecker delta tensor (1 if subscripts *i, j* are the same and 0 otherwise). The subscript *i* indicates the direction and *i* = 1, 2, 3 denote *x, y, z*, respectively, with *j* and *m* having the same meaning as *i*. The Reynolds stress (−ρ*u<sub>i</sub>' u<sub>j</sub>'*) has the superscripts ' and—denoting the turbulent fluctuating component and Reynolds time-averaged component. The total energy *E* equation is given by (6), with *h* being the enthalpy. The deviatoric stress tensor (τ<sub>*ij*</sub>)<sub>*eff*</sub> is given by Equation (7), where μ<sub>*eff*</sub> is the effective viscosity.

$$E = h - \frac{p}{\rho} + \frac{u^2}{2} \tag{6}$$

$$(\tau_{ij})_{eff} = \mu_{eff} \left( \frac{\partial u_j}{\partial x_i} + \frac{\partial u_i}{\partial x_j} \right) - \frac{2}{3} \mu_{eff} \frac{\partial u_i}{\partial x_i} \delta_{ij} \tag{7}$$

**Table 4.** Summary of solver parameters.

| Parameter                  | Value                                 |
|----------------------------|---------------------------------------|
| Solver                     | Pressure-based (segregated) [19,31]   |
| Pressure–Velocity coupling | SIMPLE [14,16]                        |
| Spatial discretization     | Second-order/second-order UPWIND [31] |
| Temporal discretization    | Second-order implicit [32]            |
| Gradient discretization    | Least-squares cell-based              |

To achieve smoothness, a value of  $10^{-4}$  was assumed as the general convergence criterion, and a value of  $10^{-6}$  was assumed for the energy equation.

#### 2.4. Validation

In general, the validation showed good results. As in the simulation made by D. Melideo et al. [23], there was a small overestimation of the temperatures of the gas (Figure 2) and aluminum (Figure 3) in relation to the experiment. Adding the fact that the temperature increase profile very closely follows that of [23], it is possible to conclude that the choices made in the preprocessing and solver were correct.

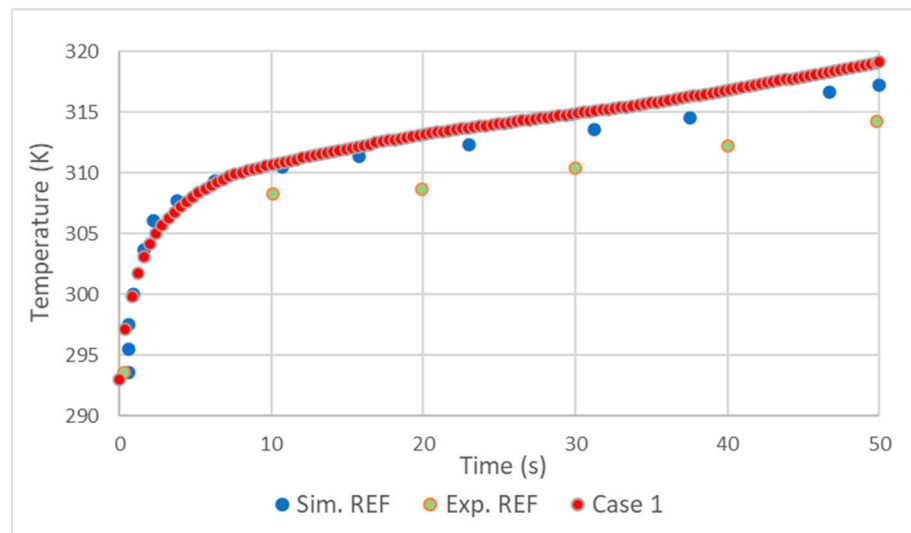


**Figure 2.** Comparison of hydrogen temperature results with REF D. Melideo et al. [23].

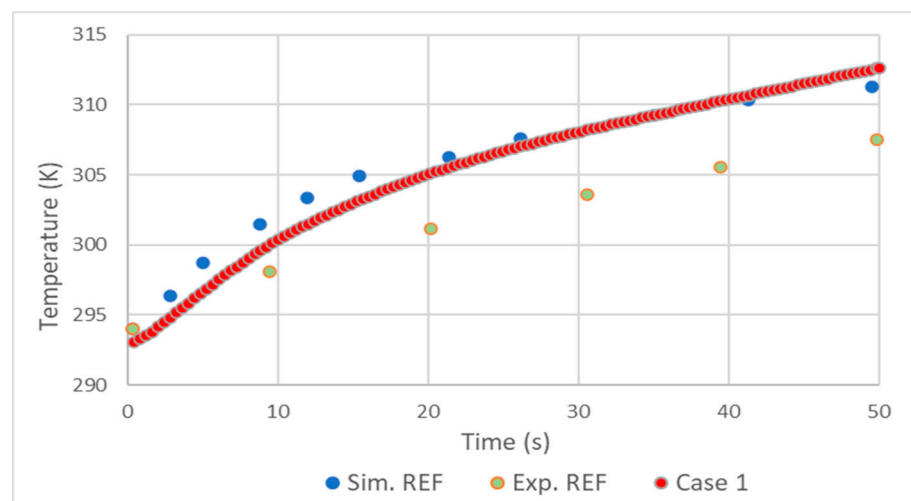


**Figure 3.** Comparison of aluminum liner temperature results with REF D. Melideo et al. [23].

The difference between simulations and experience may be explained by the effects produced by opening the valve at the beginning of filling. As with [23], in this work, higher temperatures were also found in the tank materials on the side opposite to the inlet (Figure 4). This was due to several factors, such as the effects of compression being felt more in this area and an even higher coefficient of heat transfer resulting from higher velocities.

The realizable model in case 2 closely followed the standard results, as can be seen in Table 5. However, as it presented a relatively small overestimation in temperature values, the standard model was chosen for the remaining simulations.

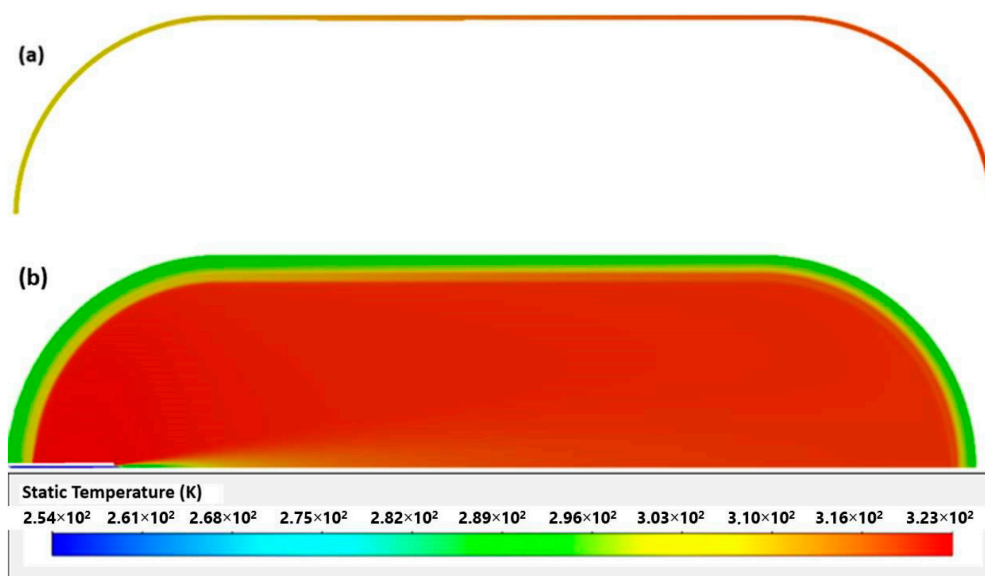


Figure 4. Temperatures of aluminum liner (a) and whole tank (b).

Table 5. Difference in temperatures between models.

|                   | Hydrogen Final Temperature (K) | Aluminum Liner Final Temperature (K) |
|-------------------|--------------------------------|--------------------------------------|
| Realizable case 2 | 320.177                        | 313.118                              |
| Standard case 1   | 319.104                        | 312.633                              |

The difference between the maximum pressure (inlet) and minimum pressure (inside the tank) throughout the filling simulations was also analyzed to verify the impact of the Joule–Thomson effect. This effect is responsible for increasing the hydrogen temperature from 2.64 °C to 5.05 °C for a pressure difference of 10 MPa [32,33]. In the current cases, the maximum difference measured was 0.19 MPa, so this effect was negligible in the current study. This is due to the fact that in the simulation, only the flow after the inlet was considered, and in this position, the pressure variation between the tank and inlet was small, decreasing even further as filling progressed [34].

### 3. Results

#### 3.1. Increase in Temperatures in Total Equilibrium with Environment

In case 3, a condition of initial equilibrium (the same initial temperature for the hydrogen, tank liner/laminate, exterior (convention condition), and the inlet) was simulated by increasing all these temperatures by 10 K, resulting in an increase in the average hydrogen final temperature of 11 K, as shown in Figure 5. This value is close to the 10 K value found by J. Zheng et al. [16] in a simulation of a type 3 tank of 70 MPa and with variable pressure conditions in the inlet. The discrepancy between values may be due to the properties of the tank materials, different volume (74 L), or the inlet pressure condition. However, it is possible to conclude that these three factors will not significantly influence the value of the linear increase in hydrogen temperature in this type of tank.

As can be seen in Figure 5, the temperature of the aluminum lining also increased linearly with the same value of 11 K, despite the different growth profile. The temperature difference between hydrogen and aluminum was approximately 10 to 12 K. The increase in the initial equilibrium temperature and consecutively lower density of hydrogen resulted in linear increases in the final pressure, initial velocity, and final velocity, according to Table 6.

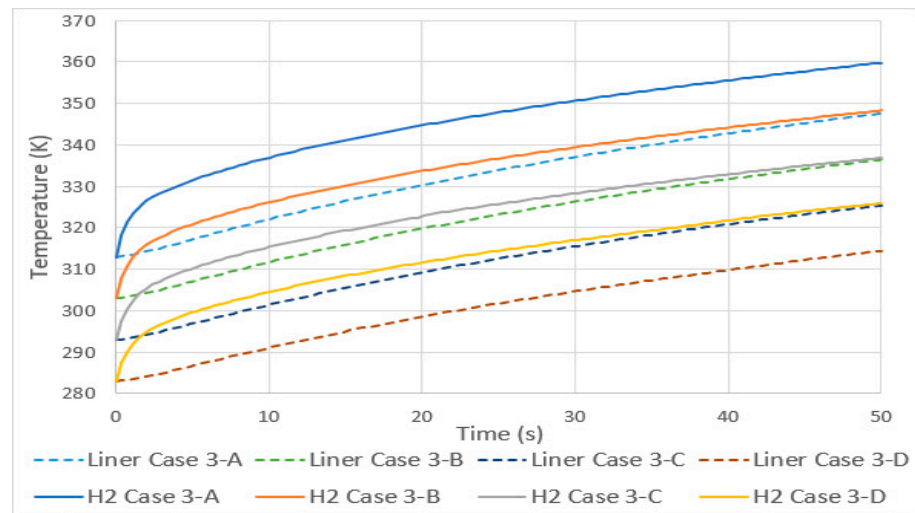


Figure 5. Hydrogen and aluminum liner temperature history for case 3.

Table 6. Maximum values of pressure and velocities for case 3.

|          | Final Pressure (MPa) | Initial Velocity (m·s <sup>-1</sup> ) | Final Velocity (m·s <sup>-1</sup> ) |
|----------|----------------------|---------------------------------------|-------------------------------------|
| Case 3-A | 19                   | 769                                   | 100.5                               |
| Case 3-B | 18.5                 | 746                                   | 100                                 |
| Case 3-C | 18                   | 723                                   | 99.5                                |
| Case 3-D | 17.5                 | 700                                   | 99                                  |

3.2. Increase in Temperature of Inlet with Fixed Equilibrium Temperature Set

In case 4, the initial temperature of the tank and hydrogen was set at 279 K (an arbitrary value to simulate a situation of lower temperatures due to the decompression of hydrogen during consumption), and the inlet and exterior were increased by 10 K per case. As in case 3, a linear relationship was found in the average gas temperature. In this case, as shown in Figure 6, the rise was 4.5 K for every 10 increases. As in the previous case, the aluminum lining also increased linearly with the same value of average temperature.

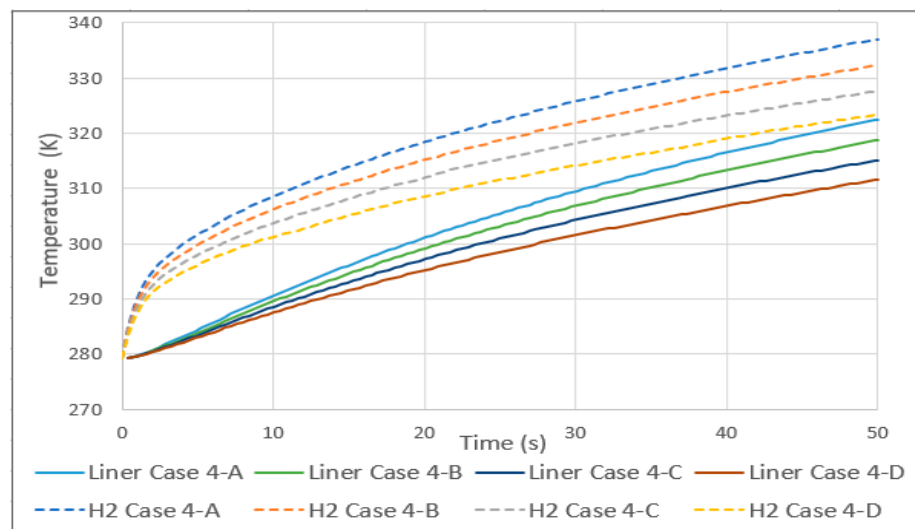


Figure 6. Hydrogen and aluminum liner temperature history for case 4.

### 3.3. Influence of Mass Flow Variation on Inlet Velocity and Temperature

As expected, the decrease in mass flow resulted in a decrease in velocity [18]; however, it was found that there was a convergence of speeds over time, Figure 7.

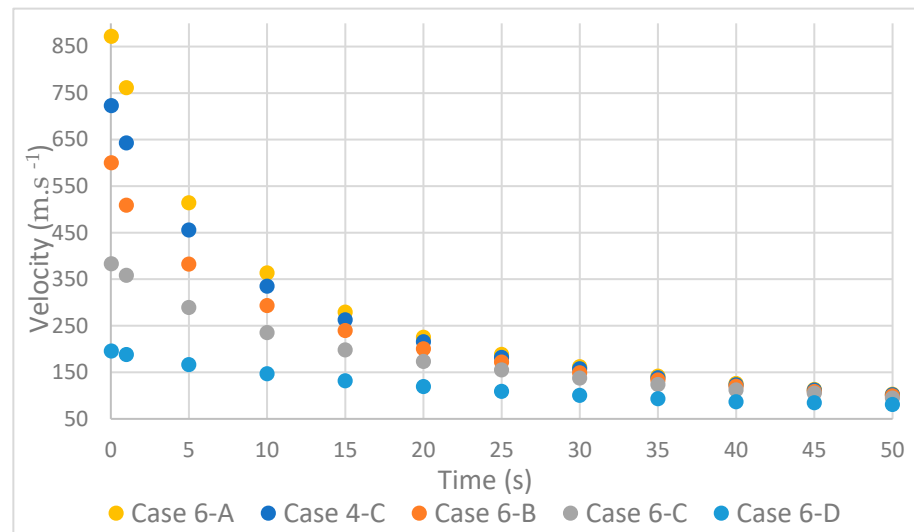


Figure 7. Variation in velocity with mass flow rate.

The hydrogen velocity also had a significant influence on the static temperature  $T$  in the inlet pipe area. This happens because in the mass flow inlet boundary condition, the imposed temperature is the total  $T_0$ , according to Equation (8) of isentropic flow.

$$\frac{T_0}{T} = 1 + \frac{\gamma - 1}{2} M^2, \quad (8)$$

with  $\gamma$  being the ratio of specific heat at constant pressure  $C_p$  and of specific heat at constant volume  $C_v$ . The Mach number,  $M$ , is given by Equation (9).

$$M = \frac{v}{a} \quad (9)$$

with  $v$  being the local fluid velocity and  $a$  being the speed of sound [35]. As the flow of a liquid can be considered incompressible due to its low variation in density, in a gas, this assumption is more restricted. The flow of a gas is considered incompressible if its Mach value is less than 0.3 and compressible otherwise [36]. In the compressible range, it is considered subsonic up to values of 1 and supersonic from 1 to 5. As the Mach number increases, the compressive effects become more evident, especially when the density is above a Mach value equal to 1. As shown in Figure 8, some of the tested cases had Mach values greater than 0.3. This is the reason why the static temperatures at the inlet and along the pipe differed from those defined in the total temperature inlet condition. As the flow in the inlet had compressible Mach, the static temperature in this zone was lower than the total.

As the supply time progresses, the static inlet temperature will converge with the total temperature. It should be emphasized that 0.3 is a general rule of thumb where the effects on the gas flow are small enough to be considered incompressible. But as can be seen in Figure 8, the effect on the temperature at the inlet still has significance until Mach 0.1. An important aspect of this is that, depending on the measuring point in the tank, the choice of the type of temperature sensor can make a difference. Now, to comply with the inlet condition, the sensor should measure the total temperature, but so far, to our knowledge, such information does not exist.

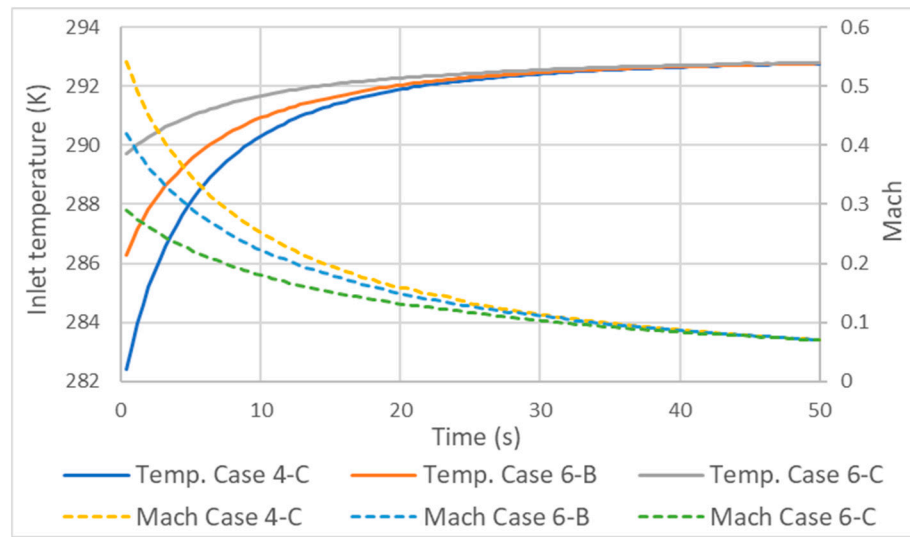


Figure 8. Variation in inlet temperature and Mach number with different mass flow rates.

3.4. Adiabatic Tank

An increase of 10 K in each simulation resulted in a sharp, nonlinear rise in temperature in cases 5 and 7. The differences in temperatures between the adiabatic cases (5 and 7) and the respective non-adiabatic cases are presented in Tables 7 and 8.

Table 7. Temperature difference between case 5 and 3.

|                  | 5-A and 3-B (303 K) | 5-B and 3-C (293 K) | 5-C and 3-D (283 K) |
|------------------|---------------------|---------------------|---------------------|
| Temperatures (K) | +56                 | +54                 | +52                 |

Table 8. Difference in temperatures between case 7 and 4-C/6.

|                  | 7-A and 4-C (8 g/s) | 7-B and 6-B (6 g/s) | 7-C and 6-C (4 g/s) |
|------------------|---------------------|---------------------|---------------------|
| Temperatures (K) | +60                 | +61                 | +60                 |

It can be verified that when materials were removed from the tank, there was a drastic rise in temperature. This occurred because aluminum begins to absorb and conduct heat from hydrogen from the beginning, thus reducing its temperature. The results demonstrate that considering a fully adiabatic tank led to a high temperature overestimation. A similar conclusion was drawn by [32,33]. Unlike the respective non-adiabatic cases, cases 5 and 7 did not show hydrogen homogeneity within the tank. As can be seen in Figure 9, there are visibly higher temperatures in the left area than in the rest of the tank. The reason for the above may be related to the low velocity, which entails low mixing with the remaining gas.

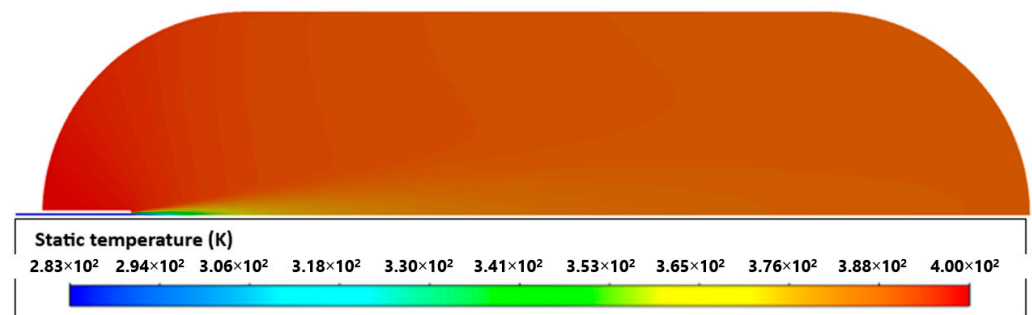


Figure 9. Adiabatic tank.

### 3.5. Tank Type 4

As expected, the hydrogen temperatures of a type 4 tank compared to type 3 are higher, Figure 10. This is due to the fact that the HDPE liner has lower thermal conductivity than aluminum. Unlike cases 3 and 4, here, the difference between the gas temperatures is not of the same magnitude as that of the lining. The difference between hydrogen temperatures at 50 s was greater than 20 K and that of the lining did not reach 5 K, the reason being, again, the low conductivity of HDPE compared to aluminum.

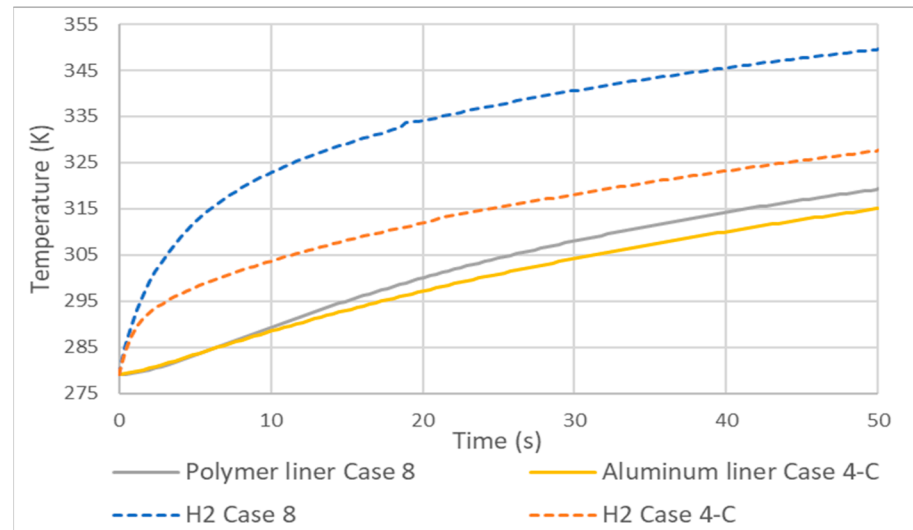


Figure 10. Temperature increase in type 3 (case 4) and 4 (case 8) tanks.

Figure 11 shows that the hydrogen pressure in tank 4 began to increase more quickly as the filling progressed. However, the velocity did not present this behavior and closely followed the velocity profile of the type 3 tank, with a maximum difference of  $20 \text{ m}\cdot\text{s}^{-1}$  at 10 s.

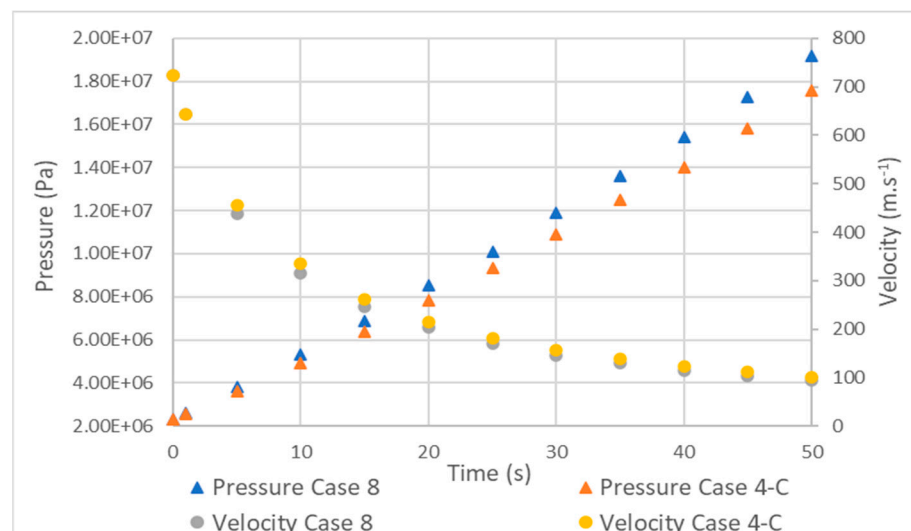


Figure 11. Comparison between pressure and velocity in type 3 (case 4) and 4 (case 8) tanks.

## 4. Conclusions

The present work aimed to carry out numerical simulations in a type 3 tank of 70 MPa normal working pressure (NWP) and constant flow rate condition to analyze the influence of key parameters such as inlet and initial temperature, mass flow rate, and material

properties on the evolution of temperature, pressure, and velocity. From the results, it is possible to conclude the following:

- The realizable model results were close to those of the standard, with the standard presenting slightly better results.
- A linear increase in the temperature of hydrogen occurred, both for tanks with a variable total initial thermal equilibrium and with a fixed initial tank temperature. An increase of 10 K resulted, in case 3, in an increase of 11 K in the average temperature, and in case 4, it resulted in an increase of 4.5 K.
- Due to the compressive nature of the flow, the variation in mass flow rate and, consequently, in velocity has significant implications for temperatures along the inlet tube. As the velocity increases, the difference between the static and total temperature increases and the static temperature decreases.
- Adiabatic tanks cause temperature increases in the order of 50 to 60 K relative to their non-adiabatic counterparts.
- The comparison between a type 3 and 4 tank, with the same conditions except for the lining, showed that the increase in temperature in the type 4 tank began to be significant at around 3 s and stabilized at around 30. The pressure was also greatly affected, while the velocity did not show relevant differences.
- It was also found that the Joule–Thomson effect was negligible for the current cases. The pressure difference found in the simulations was very small, resulting in a theoretical change in temperature of the centesimal order.

**Author Contributions:** J.M.M.: investigation, writing—original draft preparation, software; L.R.: conceptualization, supervision, writing—review and editing; G.F.P.: supervision, writing—review and editing, software, validation; J.M.: writing—review; A.B. formal analysis, software, validation, project administration. All authors have read and agreed to the published version of the manuscript.

**Funding:** This research received no external funding.

**Data Availability Statement:** Data is contained within the article.

**Conflicts of Interest:** The authors declare no conflicts of interest.

## Abbreviations

### Acronyms

|                                 |   |
|---------------------------------|---|
| NWP                             | Normal working pressure   |
| SAE                             | Society of Automotive Engineers   |
| SOC                             | State of charge   |
| CFD                             | Computational fluid dynamics  |
| UDF                             | User-defined function   |
| HDPE                            | High-density polyethylene   |
| 2D, 3D                          | Two-dimensional, three-dimensional  |
| C <sub>p</sub>                  | Specific heat at constant pressure  |
| p                               | Pressure  |
| T                               | Temperature   |
| R                               | Universal gas constant of a perfect gas                                   |
| V                               | Volume  |
| a, b                            | Constants to correct for the attractive potential of molecules and volume |
| e                               | Turbulent dissipation rate  |
| C <sub>μ</sub> , C <sub>1</sub> | Constants   |
| REF                             | Reference paper for validation  |
| M                               | Mach number   |
| γ                               | Specific heat ratio   |
| V                               | Local velocity  |
| a                               | Speed of sound  |
| δ <sub>ij</sub>                 | Kronecker delta   |
| μ                               | Viscosity   |

## Subscripts

|       |                                  |
|-------|----------------------------------|
| m     | Molar                            |
| c     | Critical                         |
| 0     | Total                            |
| i,j,k | Direction subscripts             |
| eff   | Effective                        |
| t     | Turbulent                        |
| '     | Turbulent fluctuating component  |
| –     | Reynolds time-averaged component |

## References

- Hall, C.A.S.; Klitgaard, K.A. *Energy and the Wealth of Nations*, 2nd ed.; Springer: New York, NY, USA, 2012.
- Energy Information Administration. *International Energy Outlook 2019*; Office of Energy Analysis U.S. Department of Energy: Washington, DC, USA, 2019.
- Dawood, F.; Anda, M.; Shafiullah, G.M. Hydrogen production for energy: An overview. *Int. J. Hydrogen Energy* **2020**, *7*, 3847–3869. [[CrossRef](#)]
- Schneider, J.; Meadows, G.; Mathison, S.; Veenstra, M.; Shim, J.; Immel, R.; Wistoft-Ibsen, M.; Quong, S.; Greisel, M.; McGuire, T.; et al. Validation and Sensitivity Studies for SAE J2601, the Light Duty Vehicle Hydrogen Fueling Standard. *SAE Int. J. Altern. Power*. **2014**, *53*, 257–309. [[CrossRef](#)]
- Baptista, A.; Pinho, C.; Pinto, G.; Ribeiro, L.; Monteiro, J.; Santos, T. Assessment of an Innovative Way to Store Hydrogen in Vehicles. *Energies* **2019**, *12*, 1762. [[CrossRef](#)]
- Pinto, G.; Monteiro, J.; Baptista, A.; Ribeiro, L.; Leite, J. Study of the Permeation Flowrate of an Innovative Way to Store Hydrogen in Vehicles. *Energies* **2021**, *14*, 6299. [[CrossRef](#)]
- Ribeiro, L.; Pinto, G.F.; Baptista, A.; Monteiro, J. Study on a New Hydrogen Storage System—Performance, Permeation, and Filling/Refilling. In *Hydrogen Electrical Vehicles*, 1st ed.; Sankir, M., Sankir, N., Eds.; Scrivener Publishing LLC.: Beverly, MA, USA, 2023; Volume 1, pp. 11–46.
- Suryan, A.; Kim, H.D.; Setoguchi, T. Comparative study of turbulence models performance for refueling of compressed hydrogen tanks. *Int. J. Hydrogen Energy* **2013**, *22*, 9562–9569. [[CrossRef](#)]
- Cheng, Q.; Zhang, R.; Shi, Z.; Lin, J. Review of common hydrogen storage tanks and current manufacturing methods for aluminium alloy tank liners. *Int. J. Lightweight Mater. Manuf.* **2024**, *7*, 269–284. [[CrossRef](#)]
- Li, M.; Bai, Y.; Zhang, C.; Song, Y.; Jiang, S.; Grouset, D.; Zhang, M. Review on the research of hydrogen storage system fast refueling in fuel cell vehicle. *Int. J. Hydrogen Energy* **2019**, *21*, 10677–10693. [[CrossRef](#)]
- Su, Y.; Lv, H.; Zhou, W.; Zhang, C. Review of the Hydrogen Permeability of the Liner Material of Type IV On-Board Hydrogen Storage Tank. *World Electr. Veh. J.* **2021**, *3*, 130. [[CrossRef](#)]
- Hirofani, R.; Terada, T.; Tamura, Y.; Mitsuiishi, H.; Watanabe, S. *Thermal Behavior in Hydrogen Storage Tank for Fuel Cell Vehicle on Fast Filling*; Japan Automobile Research Institute: Tokyo, Japan, 2007; 10p.
- Kim, S.C.; Lee, S.H.; Yoon, K.B. Thermal characteristics during hydrogen fueling process of type IV cylinder. *Int. J. Hydrogen Energy* **2010**, *13*, 6830–6835. [[CrossRef](#)]
- Zhao, Y.; Liu, G.; Liu, Y.; Zheng, J.; Chen, Y.; Zhao, L.; Guo, J.; He, Y. Numerical study on fast filling of 70 MPa type III cylinder for hydrogen vehicle. *Int. J. Hydrogen Energy* **2012**, *22*, 17517–17522. [[CrossRef](#)]
- Liu, Y.-L.; Zhao, Y.-Z.; Zhao, L.; Li, X.; Chen, H.-G.; Zhang, L.-F.; Zhao, H.; Sheng, R.-H.; Xie, T.; Hu, D.-H.; et al. Experimental studies on temperature rise within a hydrogen cylinder during refueling. *Int. J. Hydrogen Energy* **2010**, *7*, 2627–2632. [[CrossRef](#)]
- Zheng, J.; Guo, j.; Yang, J.; Zhao, Y.; Zhao, L.; Pan, X.; Ma, J.; Zhang, L. Experimental and numerical study on temperature rise within a 70 MPa type III cylinder during fast refueling. *Int. J. Hydrogen Energy* **2013**, *25*, 10956–10962. [[CrossRef](#)]
- Galassi, M.C.; Baraldi, D.; Iborra, B.A.; Moretto, P. CFD analysis of fast filling scenarios for 70 MPa hydrogen type IV tanks. *Int. J. Hydrogen Energy* **2012**, *8*, 6886–6892. [[CrossRef](#)]
- Miguel, N.; Acosta, B.; Moretto, P.; Cebolla, R.O. Influence of the gas injector configuration on the temperature evolution during refueling of on-board hydrogen tanks. *Int. J. Hydrogen Energy* **2016**, *42*, 19447–19454. [[CrossRef](#)]
- Kesana, N.R.; Welahettige, P.; Hansen, P.M.; Ulleberg, Ø.; Vågsæther, K. Modelling of fast fueling of pressurized hydrogen tanks for maritime applications. *Int. J. Hydrogen Energy* **2023**, *79*, 30804–30817. [[CrossRef](#)]
- Melideo, D.; Baraldi, D.; Galassi, M.C.; Cebolla, R.O.; Iborra, B.A.; Moretto, P. CFD model performance benchmark of fast filling simulations of hydrogen tanks with pre-cooling. *Int. J. Hydrogen Energy* **2014**, *9*, 4389–4395. [[CrossRef](#)]
- Wang, G.; Zhou, J.; Hu, S.; Dong, S.; Wei, P. Investigations of filling mass with the dependence of heat transfer during fast filling of hydrogen cylinders. *Int. J. Hydrogen Energy* **2014**, *9*, 4380–4388. [[CrossRef](#)]
- Ortiz Cebolla, R.; Acosta, B.; de Miguel, N.; Moretto, P. Effect of precooled inlet gas temperature and mass flow rate on final state of charge during hydrogen vehicle refueling. *Int. J. Hydrogen Energy* **2015**, *40*, 4698–4706. [[CrossRef](#)]
- Melideo, D.; Baraldi, D.; Iborra, B.A.; Cebolla, R.O.; Moretto, P. CFD simulations of filling and emptying of hydrogen tanks. *Int. J. Hydrogen Energy* **2017**, *11*, 7304–7313. [[CrossRef](#)]
- ANSYS. *ANSYS Fluent User Guide*; Ansys Fluent; Ansys: Canonsburg, PA, USA, 2022.

25. AIAA. *Guide for the Verification and Validation of Computational Fluid Dynamics Simulations (AIAA G-077-1998(2002))*; American Institute of Aeronautics and Astronautics, Inc.: Washington, DC, USA, 1998.
26. Miguel, N.; Cebolla, R.O.; Acosta, B.; Moretto, P.; Harskamp, F.; Bonato, C. Compressed hydrogen tanks for on-board application: Thermal behaviour during cycling. *Int. J. Hydrogen Energy* **2015**, *19*, 6449–6458. [[CrossRef](#)]
27. Suryan, A.; Kim, H.D.; Setoguchi, T. Three dimensional numerical computations on the fast filling of a hydrogen tank under different conditions. *Int. J. Hydrogen Energy* **2012**, *9*, 7600–7611. [[CrossRef](#)]
28. Nasrifar, K. Comparative study of eleven equations of state in predicting the thermodynamic properties of hydrogen. *Int. J. Hydrogen Energy* **2010**, *8*, 3802–3811. [[CrossRef](#)]
29. Kim, M.-S.; Ryu, J.-H.; Oh, S.-J.; Yang, J.-H.; Choi, S.-W. Numerical Investigation on Influence of Gas and Turbulence Model for Type III Hydrogen Tank under Discharge Condition. *Energies* **2020**, *23*, 6432. [[CrossRef](#)]
30. Magi, V.I.J.A.V. The k- $\epsilon$  Model and computed spreading rates in round and plate jets. *Numer. Heat Transf. A Appl.* **2001**, *4*, 317–334.
31. Kim, M.-S.; Jeon, H.-K.; Lee, K.-W.; Ryu, J.-H.; Choi, S.-W. Analysis of Hydrogen Filling of 175 Liter Tank for Large-Sized Hydrogen Vehicle. *Appl. Sci.* **2022**, *12*, 4856. [[CrossRef](#)]
32. Galassi, M.C.; Papanikolaou, E.; Heitsch, M.; Baraldi, D.; Iborra, B.A.; Moretto, P. Assessment of CFD models for hydrogen fast filling simulations. *Int. J. Hydrogen Energy* **2014**, *11*, 6252–6260. [[CrossRef](#)]
33. Miguel, N.; Acosta, B.; Baraldi, D.; Melideo, R.; Cebolla, R.O.; Moretto, P. The role of initial tank temperature on refuelling of on-board hydrogen tanks. *Int. J. Hydrogen Energy* **2016**, *20*, 8606–8615. [[CrossRef](#)]
34. Acosta, B.; Moretto, P.; Miguel, N.; Ortiz, R.; Harskamp, F.; Bonato, C. JRC reference data from experiments of on-board hydrogen tanks fast filling. *Int. J. Hydrogen Energy* **2014**, *35*, 20531–20537. [[CrossRef](#)]
35. Glenn Research Center. *Speed of Sound*; NASA: Washington, DC, USA, 2021. Available online: <https://www.grc.nasa.gov/www/BGH/snddrv.html> (accessed on 14 June 2023).
36. Ansys. *ANSYS Fluent Theory Guide*; Ansys Fluent; Ansys: Canonsburg, PA, USA, 2022.

**Disclaimer/Publisher’s Note:** The statements, opinions and data contained in all publications are solely those of the individual author(s) and contributor(s) and not of MDPI and/or the editor(s). MDPI and/or the editor(s) disclaim responsibility for any injury to people or property resulting from any ideas, methods, instructions or products referred to in the content.